Published in

Applied Surface Science 255 (2008) 2551–2556

Comparative surface and nano-tribological characteristics of nanocomposite diamond-like carbon thin films doped by silver

H.-S. Zhang[1,*], J. L. Endrino[2,3], A. Anders[3]

[1]*Department of Mechanical Engineering, University of California, Berkeley, CA 94720*
[2]*Instituto de Ciencias de Materiales de Madrid, E-28049, Madrid, Spain*
[3]*Lawrence Berkeley National Laboratory, Berkeley, CA 94720*

Comparative surface and nano-tribological characteristics of nanocomposite diamond-like carbon thin films doped by silver

H.-S. Zhang[1,*], J. L. Endrino[2,3], A. Anders[3]

[1]*Department of Mechanical Engineering, University of California, Berkeley, CA 94720*
[2]*Instituto de Ciencias de Materiales de Madrid, E-28049, Madrid, Spain*
[3]*Lawrence Berkeley National Laboratory, Berkeley, CA 94720*

Abstract

In this study we have deposited silver-containing hydrogenated and hydrogen-free diamond-like carbon (DLC) nanocomposite thin films by plasma immersion ion implantation-deposition methods. The surface and nano-tribological characteristics were studied by x-ray photoelectron spectroscopy (XPS), atomic force microscopy (AFM) and nano-scratching experiments. The silver doping was found to have no measurable effect on sp^2-sp^3 hybridization of the hydrogenated DLC matrix and only a slight effect on the hydrogen-free DLC matrix. The surface topography was analyzed by surface imaging. High- and low-order roughness determined by AFM characterization was correlated to the DLC growth mechanism and revealed the smoothing effect of silver. The nano-tribological characteristics were explained in terms of friction mechanisms and mechanical properties in correlation to the surface characteristics. It was discovered that the adhesion friction was the dominant friction mechanism; the adhesion force between the scratching tip and DLC surface was decreased by hydrogenation and increased by silver doping.

*Corresponding Author: Tel: (510) 642-3270; Fax: (510) 643-5599; E-mail: hszhang@me.berkeley.edu

Submitted to *Applied Surface Science* on April 10th, 2008; revised manuscript submitted on July 29th, 2008

1. Introduction

Diamond-like carbon (DLC) coatings have attracted significant research attention for their wide applications as protective layers because of their high strength, low roughness and excellent tribological properties. Recently composite DLC-metal coatings, especially DLC-Ag, have gained increasing attention as a new area of DLC research. Due to the amorphous nature of DLC, metallic species can be doped into DLC coatings to form nanocomposites with special functionalities, with only small effect on DLC's good mechanical and tribological properties. For example, in biomedical research, minute silver concentration is highly toxic to germs while relatively non-toxic to human cells [1-6]. In optical device application, multilayer coatings of DLC/Ag-alloy can be made transparent and have low emissivity which make them attractive for window applications [7]. It has been suggested that the doping of DLC with silver may also be used as coating materials for electrodes in electrochemical analysis in microelectromechanical systems [8]. As protective layer, DLC-Ag has demonstrated low coefficient of friction and high wear resistance [6,9,10].

While the effect of adding silver to DLC coatings has been tested to be beneficial in a variety of applications, the surface and nano-tribological properties of these films are not yet completely understood. In order to justify the application of DLC-Ag nanocomposite thin films in various applications, in this study surface analysis and nano-tribological testing were carried out ex-situ for DLC-Ag nanocomposite thin films deposited by plasma immersion ion implantation-deposition (PIII-D) methods. Clearly the effect of surface chemistry and topography can affect the nano-tribological properties of thin films; therefore the relevance of such change with respect to the effect of hydrogenation has been analyzed by comparing the effect of silver addition in both hydrogenated and hydrogen-free DLC. Besides hydrogenation,

another important variable that can significantly affect the nano-tribological behaviors of DLC is the sp^2/sp^3 carbon bonding ratio in the DLC network. In the past it has been very difficult to separate the effect of hydrogenation, metal doping and sp^2/sp^3 ratio. In this study we overcame such limitation by the use of "selective bias" PIII-D techniques which allowed us varying the doping of metal element and the hydrogen content in the films without significantly modifying the sp^2/sp^3 ratio [11]. In this paper the notation of a-C:H and a-C are referred to hydrogenated and hydrogen-free DLC; the corresponding silver-containing samples are referred to a-C:H/Ag and a-C/Ag. X-ray photoelectron spectroscopy (XPS) was used to analyze the chemistry of the top surface layer; atomic force microscopy (AFM) was used to characterize the surface topography; and mechanical tests of nano-scratching were carried out to determine the nano-tribological characteristics.

2. Experimental

In order to study the hydrogenation and silver doping effects on the surface and nano-tribological properties of the DLC films, four samples were deposited and tested: a-C:H, a-C:H/Ag, a-C and a-C/Ag. The DLC-Ag nanocomposite thin films were grown by PIII-D methods as follows. A thick layer of chromium was deposited firstly onto the silicon substrate as a buffer layer. The hydrogenated films were grown from a methane reactive precursor together with pulsed cathodic arc deposition using a silver cathode. Carbon and hydrogen were taken from the process gas as chemical vapor deposition (CVD) process; and silver came from the arc cathode as physical vapor deposition (PVD) process. The hydrogen-free films were grown by alternating arc pulses from two separate cathodic arc sources of carbon and silver. The feedstock materials were exclusively the two cathodes; no background gas was needed or added. The

substrates were biased with negative 1 kV pulses that were 2 μs long, with a duty cycle of 12.5%. One of the advanced features of the deposition system was that it was equipped with a computer-controlled bias amplifier that can synchronize substrate bias with the pulsing production of plasma. In order to avoid excessive re-sputtering of carbon atoms during the deposition of silver, no bias voltage was applied during the deposition of metallic component [11]. Such substrate biasing also allowed good control of sp^2/sp^3 ratio.

The four nanocomposite thin films were characterized by an XPS system (PHI 5400, Physical Electronics) equipped with a monochromatic Al-Kα (1486.6 eV) X-ray source and a spectrometer operated at pass energy of 35.75 eV and energy step of 0.05 eV at 50 ms. Each scan was repeated 20 times to take the average. The surface topography was measured by AFM (Dimension 3100, Veeco Digital Instruments) operated in tapping mode with a drive frequency of 259.332 kHz and at a scan rate of 2 Hz. For a quantitative evaluation of the surface topography, the centerline average (CLA) roughness R_a, root-mean-square (RMS) roughness R_q, skewness S, and kurtosis K were calculated from surface height data z_i obtained from 1 × 1 μm^2 AFM area scans by using numerical integration and the following relationships:

$$R_a = \frac{1}{N}\sum_{i=1}^{N}\left|z_i - \bar{z}\right|,$$

$$R_q = \left[\frac{1}{N}\sum_{i=1}^{N}\left|z_i - \bar{z}\right|^2\right]^{1/2},$$

$$S = \frac{1}{R_q^{\,3}}\frac{1}{N}\sum_{i=1}^{N}(z_i - \bar{z})^3,$$

$$K = \frac{1}{R_q^{\,4}}\frac{1}{N}\sum_{i=1}^{N}(z_i - \bar{z})^4,$$

where N is the number of surface height data (i.e. $N = 512 \times 512 = 262144$) and $\bar{z}$ is the mean-height distance. The surface nano-mechanical properties of the deposited coatings were studied

with a nano-scratching apparatus (Nanoscope II, Digital Instruments) retrofitted with a capacitive force transducer (Triboscope, Hysitron) operated in a controlled environment of temperature ~25 ^{o}C and relative humidity ~ 45 percent. The machine setup has been introduced elsewhere [12]. The nano-scratching tests were performed with a conospherical diamond tip with ~ 20 μm nominal radius; the normal loads were 10, 20, 40 and 80 μN; the scratching speed was set to 400 nm/s. Every scratch was done on a new location and along a 8 μm straight line. The coefficient of friction, $\mu = F/L$, where F is the lateral frictional force and L is the applied normal load, was calculated only for the last 4 μm scratching distance to avoid the initial static-dynamic transition instability.

3. Results and discussion

The chemical composition, sp^2- and sp^3-coordinated carbon content and microstructure of the films have been analyzed in a previous paper [1]. The silver content was measured to be 5.5±1 and 5.6±1 at.% for a-C:H/Ag and a-C/Ag, respectively. The qualitative depth-profile of hydrogen was obtained for both hydrogenated films. Other results by x-ray diffractometry (XRD) and transmission electron microscopy (TEM) have revealed that under similar deposition conditions the silver species cluster to be nano-crystalline phase in the film with grain size around 5 nm [5,9,13]. This study aims at surface properties and nano-tribological characteristics, therefore XPS and AFM exclusively give surface properties of the four samples, with the previous results as the complementary information.

The deconvoluted XPS C1*s* peaks of the four samples are shown in Fig. 1 after performing a Shirley inelastic background subtraction [14]. Four Gaussian profiles with characteristic binding energies were fitted to each C1*s* peak; each was associated with a film constituent of a certain

chemical state [15,16]. Table 1 summarizes the deconvolution details. The carbon peaks at binding energies of ~284.5 and ~285.4 eV (denoted by C1*s*-1 and C1*s*-2) correspond to sp^2- and sp^3-coordinated carbon bonding, respectively. It is noteworthy that their full width at half maximum (FWHM) increase by the silver doping. Because XPS measures the core-level electron energy, which is a quantumized value, the peak width is incurred by the measuring noise. The possible explanation of the FWHM increase by silver doping is because of the disordering of the top surface layer microstructure. The disordering of carbon due to ion bombardment has been explained in detail [17], and has also been observed in the Raman scan on the hydrogen-free DLC-Ag nanocomposite [1]. The sp^2 and sp^3 carbon fractions in the amorphous phases can be estimated by using deconvolution method of the C1*s* XPS spectra proposed by Jackson and Nuzzo [18] and Diaz *et al* [19]. By comparison silver doping slightly decreased the sp^3 content in hydrogen-free DLC, while for hydrogenated DLC the sp^2/sp^3 ratio was relatively constant. An explanation for the slight drop in sp^3 content in hydrogen-free DLC is due to its cathodic arc deposition process that the subplantation mechanism [20,21] was suppressed by the presence of silver [13,22]. Also, the silver species may have formed nano-particles that absorbed compressive stress from the DLC matrix to reduce the carbon densification [6]; this effect is more pronounced in hydrogen-free DLC films than hydrogenated DLC films because in hydrogenated DLC films hydrogen fills up much of the empty space of the DLC network and therefore the magnitude of compressive stress was less during deposition. The other two carbon peaks, denoted by C1*s*-3 and C1*s*-4 respectively, are associated with sp^2 and sp^3 carbon bonding with adsorbents on the coating surfaces. In Fig. 2 the silver signals reveal the presence of silver at the top surface. Because the Ag 3*d* spectra do not reveal discernible peak broadening, the silver species can be inferred to exist mostly in the metallic state [3]. This provides another

evidence to the existence of nano-crystalline silver particles in the DLC matrix in addition to the previous observations by other techniques [5,9,13].

Because this study focuses on surface and nano-tribological characteristics, the film surface characteristics rather than the film bulk properties are emphasized. The surface topographic images taken by AFM are shown in Fig. 3; the roughness values are plotted in Fig. 4. On the surface of a-C:H, the grain-like morphology was very likely because the deposited DLC followed the preexisting surface structure, reflecting the crystalline chromium feature underneath [9]. The surface morphology of a-C:H/Ag contains finer grain-like feature than a-C:H possibly because the silver species formed nano-particles that also affected the growth of the DLC. The grain-like morphology is less obvious with a-C which demonstrated certain smoothing mechanism; the smoothing was probably due to the diffusion effect of energetic carbon ions from cathodic arc. The surface of a-C/Ag is very smooth for the possible reason that energetic carbon ions and silver ions from cathodic arc interacted during deposition and the diffusion effect was enhanced. In Fig. 4, a-C/Ag shows the lowest R_a, R_q values. It is noticeable that silver doping reduced R_a, R_q values for hydrogenated film as well because the 3D-growth of silver content also has the smoothing effect [23]. The high-order roughness values reveal some difference between hydrogenated and hydrogen-free DLC coatings. The fact that $S \approx 0$, $K \approx 3$ for the hydrogenated samples tells that their surface microscale topography exhibited a Gaussian distribution, which is the result of very uniform microstructure and chemical species. The high kurtosis ($K > 5$) of hydrogen-free coatings reveals the existence of some uneven local features on the surfaces. The a-C had negative skewness while a-C/Ag had positive skewness, which reveals that their surfaces contained some dents and spikes, respectively. It is hypothesized that a-C film was slightly contaminated by macroparticles during the cathodic arc deposition which left some

pin-holes; while a-C/Ag possibly contained some silver nano-particles that made the surface of some protrusions out of the otherwise highly smooth surface. The surface morphology was also under the influence of surface energy; the hydrogenation and silver doping decreased and increased the surface energy of the DLC films, respectively, which may thermodynamically affect the surface morphology. However such effect was very small compared to the smoothing effects of energetic carbon and silver ions during the PIII-D deposition.

The nano-scratching tests with different loads on a-C:H/Ag have been plotted in Fig. 5 to show as an example of such testing. The coefficient of friction, μ, was observed to have a lower average value and less fluctuation under higher applied loads. The average value of μ, $\overline{\mu}$, decreased with applied load because they were calculated only with the measured normal and lateral forces; the adhesion force between the tip and sample surface was not counted. When the normal applied load was small, the adhesion force was comparable to the external load and raised the apparent μ value [24]. A study involving contact geometry and adhesion force predicts that μ is inversely proportional to the cubic root of the normal applied load, i.e., $\mu \propto L^{-1/3}$, where L is the applied load [25].

The $\overline{\mu}$ and the standard deviation of μ, $\sigma(\mu)$, were plotted in Fig. 6 to make a comparison between the four samples. The frictional force may come from two different mechanisms: adhesion associated with elastic deformation of the surfaces, and abrasion (plowing), which involves plastic deformation. The surface imaging by AFM after the nano-scratching tests did not yield any discernible evidence of permanent deformation, suggesting that the scratching was predominantly elastic. The $\overline{\mu}$ under high loads were less than 0.2, which is in agreement with the prediction of the classical adhesion theory of friction [26]. Generally the adhesion force is proportional to the surface energy of the two contacting surfaces, which depends on the number

of dangling bonds on the surface and the degree of surface reconstruction [27]. The vertical surface adhesion force can be modeled as $P = -\chi R\gamma\pi$, where γ is the surface energy, R is the contact asperity radius, and χ is a computation factor (χ=1.5 for the John-Kendall-Roberts model) [28,29]. It is reasonable to infer that the lateral-direction frictional force is also influenced by surface energy. Hydrogen decreases the DLC surface energy [27,30]; whereas the presence of silver on the top surface increases the surface energy [2,5,31]. Therefore the chemical composition partially explains the results that hydrogenated films had lower $\overline{\mu}$ than hydrogen-free films, and that DLC nanocomposite films doped with silver had higher $\overline{\mu}$ than pure DLC films.

The mechanical properties could also contribute to the friction difference across the samples. Under high external load, i.e. 80 μN, the plastic shearing (plowing) effect could be high and the frictional force was dependent on the materials bulk properties, such as modulus and hardness. With this mechanism, coatings of lower strength involved a larger plowing effect, and thus more frictional force [32]. The previous paper has shown that silver doping increases the strength of hydrogen-free DLC films while decreases the strength of hydrogenated DLC films [1]. However, the mechanical property effect was secondary to the surface energy effect within the load range of this study.

The low-order roughness values are usually also related to the tribological behavior. The R_a, R_q values are inversely related to $\overline{\mu}$ because low roughness induces more adhesion force by non-contacting (proximity) surface asperities [33,34]. The surface roughness effect is best illustrated by a-C/Ag which had the lowest R_a, R_q values and highest $\overline{\mu}$. Though $\sigma(\mu)$ in Fig. 9(b) was found to vary inversely with R_a, R_q values, the exact correlation could not be confirmed. There

are several reasons that may contribute to $\sigma(\mu)$, including the scratching speed, the tip-surface adhesion strength, and the magnitude of $\overline{\mu}$. Further studies of the nano-tribological properties are expected to explain the friction statistics and possible existence of wear particles.

4. Summary and Conclusions

In this study, PIII-D methods were employed to deposit hydrogenated and hydrogen-free DLC-Ag nanocomposite thin films. One method was a hybrid CVD-PVD process, leading to hydrogenated films, and the other used alternating cathodic arcs from two cathodes giving the hydrogen-free films. The comparative study of the nanocomposite thin films was carried out to determine the silver doping and hydrogenation effect on the surface and nano-tribological characteristics. The XPS results revealed slight effect of silver doping on carbon hybridization and disordering. The surface imaging, low- and high-order roughness obtained from AFM demonstrated the smoothing effect of silver, and different growth mechanism of hydrogenated and hydrogen-free DLC-Ag nanocomposite films by PIII-D method. The nano-tribological results by nano-scratching testing revealed that the adhesion friction was the dominant friction mechanism under load force less than 80 μN and with a tip of ~20 μm radius; this mechanism could have caused the inverse relationship between coefficient of friction and external applied load. This observation suggests that when the adhesion friction was dominant, the sample's mechanical properties did not contributed significantly to the friction difference across the samples; it further suggests that the adhesion force was dependent on the low-order surface roughness, and was proportional to the surface energy that was directly related to the surface chemical composition.

Acknowledgements

Work at Lawrence Berkeley National Laboratory was supported by U.S. Department of Energy under Contract No. DE-AC02-05CH11231. Financial support from the Marie Curie Outgoing Fellowship Grant MOIF-CT-2005-021951 to one of the authors (J.L.E.) is gratefully acknowledged.

References

[1] J.L. Endrino, R. Escobar Galindo, H.-S. Zhang, M. Allen, R. Gago, A. Espinosa, A. Anders, Surf. Coat. Technol. 202 (2008) 3675.

[2] I. Kleps, M. Danila, A. Angelescu, M. Miu, M. Simion, T. Ignat, A. Bragaru, L. Dumitru, G. Teodosiu, Mater. Sci. Eng. C 27 (2007) 1439.

[3] S.C.H. Kwok, W. Zhang, G.J. Wan, D.R. McKenzie, M.M.M. Bilek, P.K. Chu, Diamond Relat. Mater. 16 (2007) 1353.

[4] R. Hauert, Diamond Relat. Mater. 12 (2003) 583.

[5] M.L. Morrison, R.A. Buchanan, P.K. Liaw, C.J. Berry, R.L. Brigmon, L. Riester, H. Abernathy, C. Jin, R.J. Narayan, Diamond Relat. Mater. 15 (2006) 138.

[6] R.J. Narayan, Diamond Relat. Mater. 14 (2005) 1319.

[7] K. Chiba, T. Takahashi, T. Kageyama, H. Oda, Appl. Surf. Sci. 246 (2005) 48.

[8] H.L. Lee, J-M. Ting, Mater. Chem. Phys. 82 (2003) 567.

[9] C.P. Lungu, Surf. Coat. Technol. 200 (2005) 198.

[10] C.P. Lungu, I. Mustata, G. Musa, V. Zaroschi, A. Mihaela Lungu, K. Iwasaki, Vacuum 76 (2004) 127.

[11] A. Anders, N. Pasaja, S. Sansongsiri, Rev. Sci. Instrum. 78 (2007) 063901.

[12] W. Lu, K. Komvopoulos, J. Trib. 123 (2001) 641.

[13] G. Matenoglou, G.A. Evangelakis, C. Kosmidis, S. Foulias, D. Papadimitriou, P. Patsalas, Appl. Surf. Sci. 253 (2007) 8155.

[14] D.A. Shirley, Phys. Rev. B 5 (1972) 4709.

[15] W. Lu, K. Komvopoulos, S.W. Yeh, J. Appl. Phys. 89 (2001) 2422.

[16] D. Wan, K. Komvopoulos, J. Phys. Chem. C 111 (2007) 9891.

[17] J. Robertson, Diamond Relat. Mater. 4 (1995) 297.

[18] S.T. Jackson, R.G. Nuzzo, Appl. Surf. Sci. 90 (1995) 195.

[19] J. Diaz, G. Paolicelli, S. Ferrer, F. Comin, Phys. Rev. B 54 (1996) 8064.

[20] Y. Lifshitz, S.R. Kasi, J.W. Rabalais, W. Eckstein, Phys. Rev. B 41 (1990) 10468.

[21] Y. Lifshitz, C.D. Roux, K. Boyd, W. Eckstein, J.W. Rabalais, Nucl. Instrum. Methods Phys. Res. B 83 (1993) 351.

[22] N. Pasaja, S. Sansongsiri, S. Intarasiri, T. Vilaithong, A. Anders, Nucl. Instrum. Methods Phys. Res. B 259 (2007) 867.

[23] A. Anders, E. Byon, D.-H. Kim, K. Fukuda, S.H.N. Lim, Solid State Comm. 140 (2006) 225.

[24] S.J. Timpe, K. Komvopoulos, J. Microelectromechanical Sys. 15 (2006) 1612.

[25] K.L. Johnson, Contact Mechanics, Cambridge University Press, Cambridge, U.K. 1985.

[26] F.P. Bowden, D. Tabor, Friction and Lubrication of Solids, Part I, Clarendon Press, Oxford, U.K. 1950.

[27] S. Hong, M.Y. Chou, Phys. Rev. B 57 (1998) 6262.

[28] K.L. Johnson, K. Kendall, A.D. Roberts, Proc. Royal Society of London, Series A, Math. Phys. Sci. 324 (1971) 301.

[29] B.V. Derjaguin, V.M. Muller, Y.P. Toporov, J. Colloid and Interface Sci. 53 (1975) 314.

[30] S. Zhang, G. Wagner, S.N. Medyanik, W.-K. Liu, Y.-H. Yu, Y.-W. Chung, Surf. Coat. Technol. 177-178 (2004) 818.

[31] W. Ye, Y. Chang, C. Ma, B. Jia, G. Cao, C. Wang, Appl. Surf. Sci. 253 (2007) 3419.

[32] N.P. Suh, H.-C. Sin, Wear 69 (1981) 91.

[33] F.W. Delrio, M.P. De Boer, J.A. Knapp, E.D. Reedy Jr, P.J. Clews, M.L. Dunn. Nature Mater. 4 (2005) 629.

[34] S.J. Timpe, K. Komvopoulos, J. Microelectromechanical Sys. 14 (2005) 1356.

List of Figures

Tables

Table 1. List of the XPS deconvolution results and $sp^2/(sp^2+sp^3)$ ratios of the four samples.

Sample	C1*s*-1		C1*s*-2		C1*s*-3		C1*s*-4		Area ratio
	Position (eV)	FWHM (eV)	Position (eV)	FWHM (eV)	Position (eV)	FWHM (eV)	Position (eV)	FWHM (eV)	$sp^2/(sp^2+sp^3)$
a-C:H	284.51	1.60	285.43	1.57	286.83	1.58	288.33	1.58	0.746
a-C:H/Ag	284.65	1.70	285.76	1.71	286.95	1.64	288.65	1.65	0.730
a-C	284.55	1.64	285.48	1.64	286.68	1.64	288.42	1.64	0.667
a-C/Ag	284.40	1.72	285.48	1.72	286.88	1.62	288.30	1.68	0.744

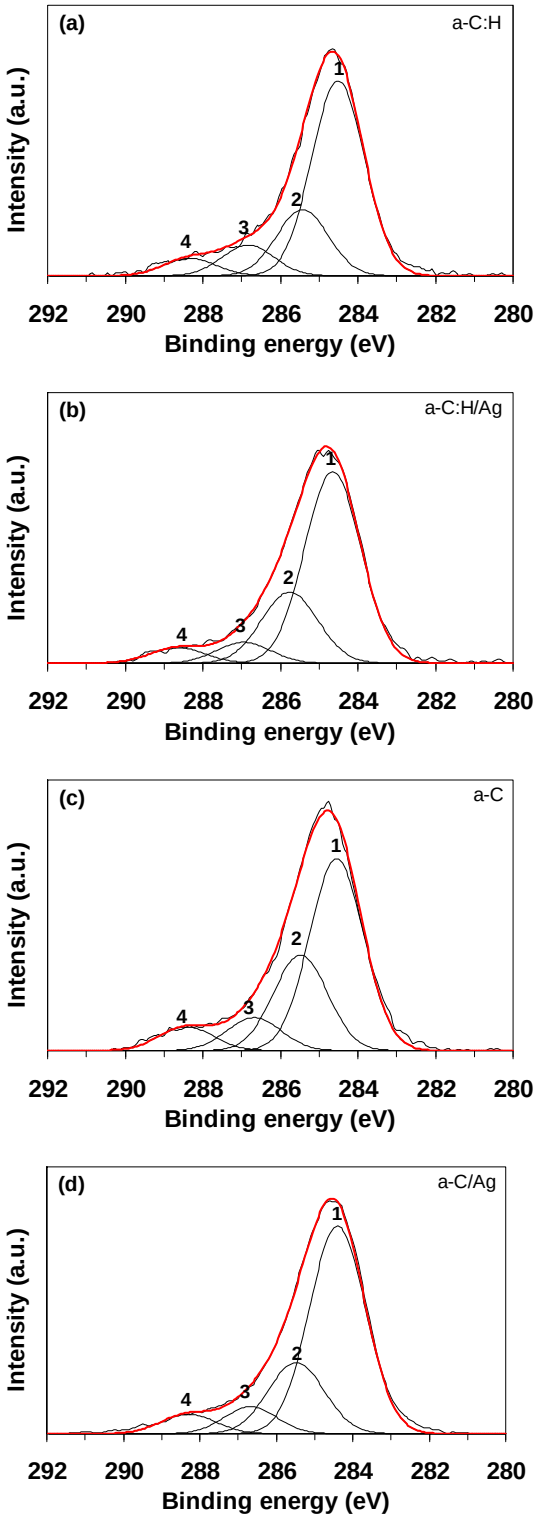
(a)
a-C:H
(b)
a-C:H/Ag
(c)
a-C
(d)
a-C/Ag
Intensity (a.u.)
Binding energy (eV)
292
290
288
286
284
282
280
1
2
3
4

Figure 1

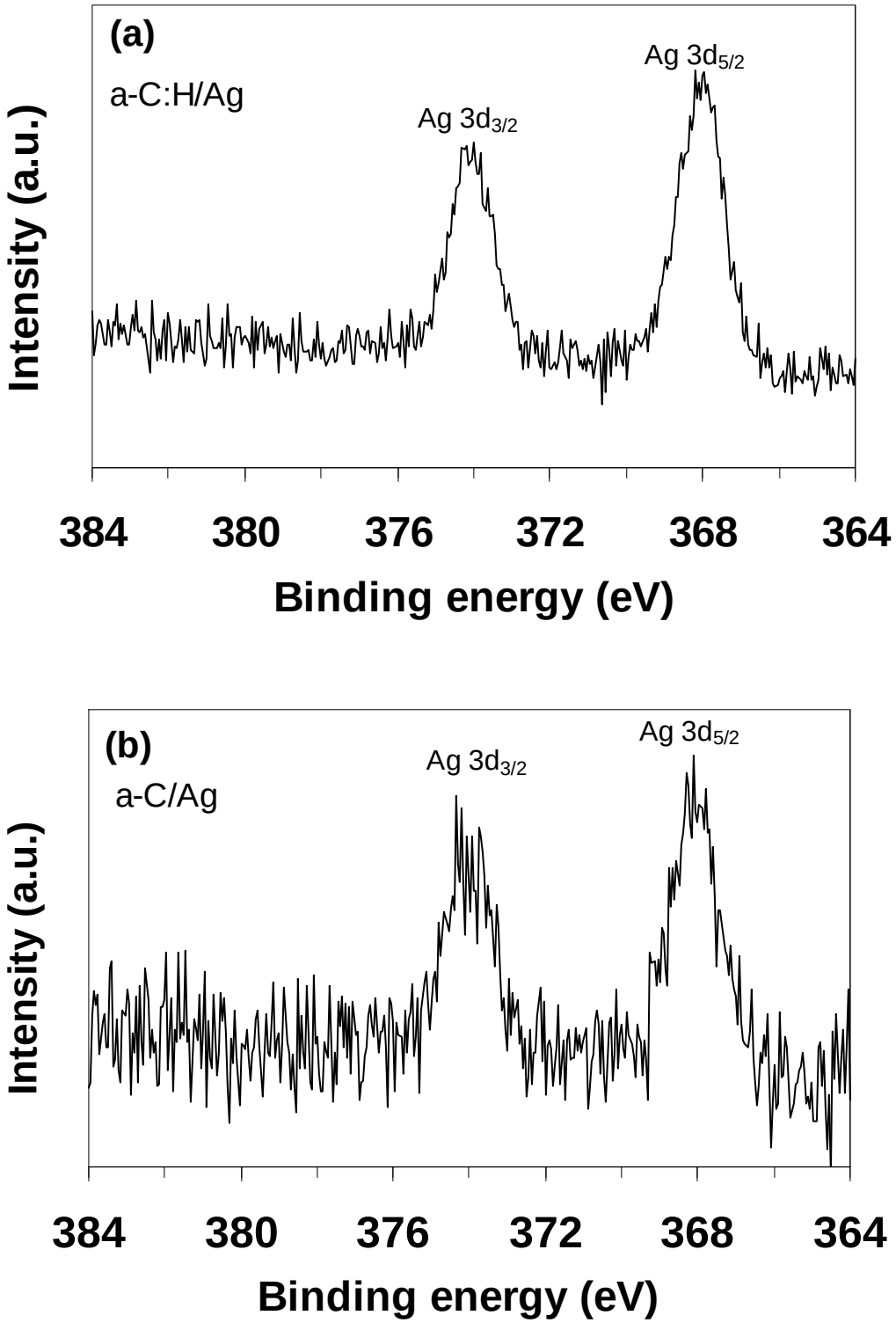
(a)
a-C:H/Ag
Ag 3d3/2
Ag 3d5/2
Intensity (a.u.)
384
380
376
372
368
364
Binding energy (eV)
(b)
a-C/Ag
Ag 3d3/2
Ag 3d5/2
Intensity (a.u.)
384
380
376
372
368
364
Binding energy (eV)

Figure 2

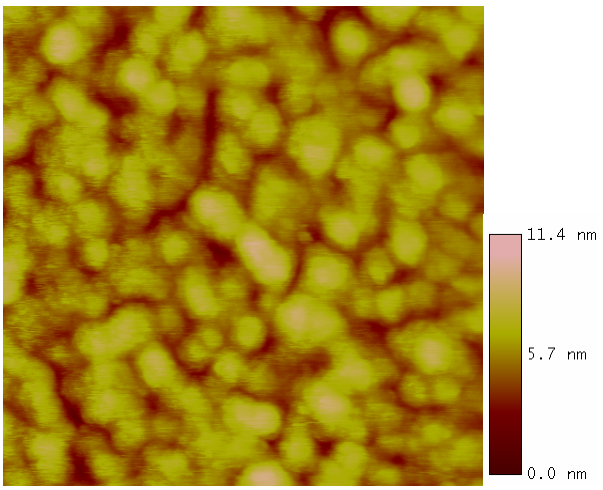

(a)

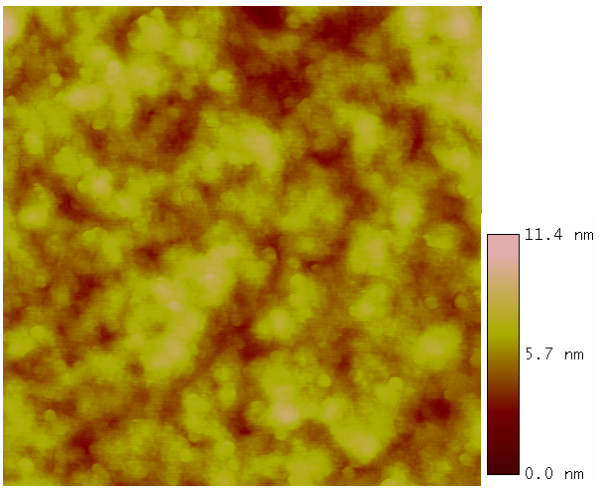

(b)

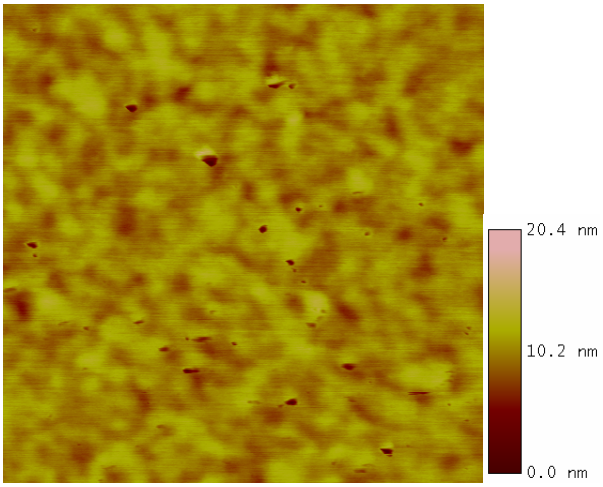

(c)

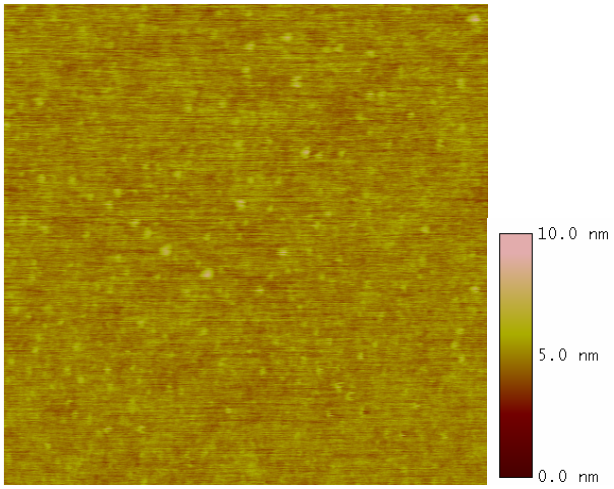

(d)

Figure 3

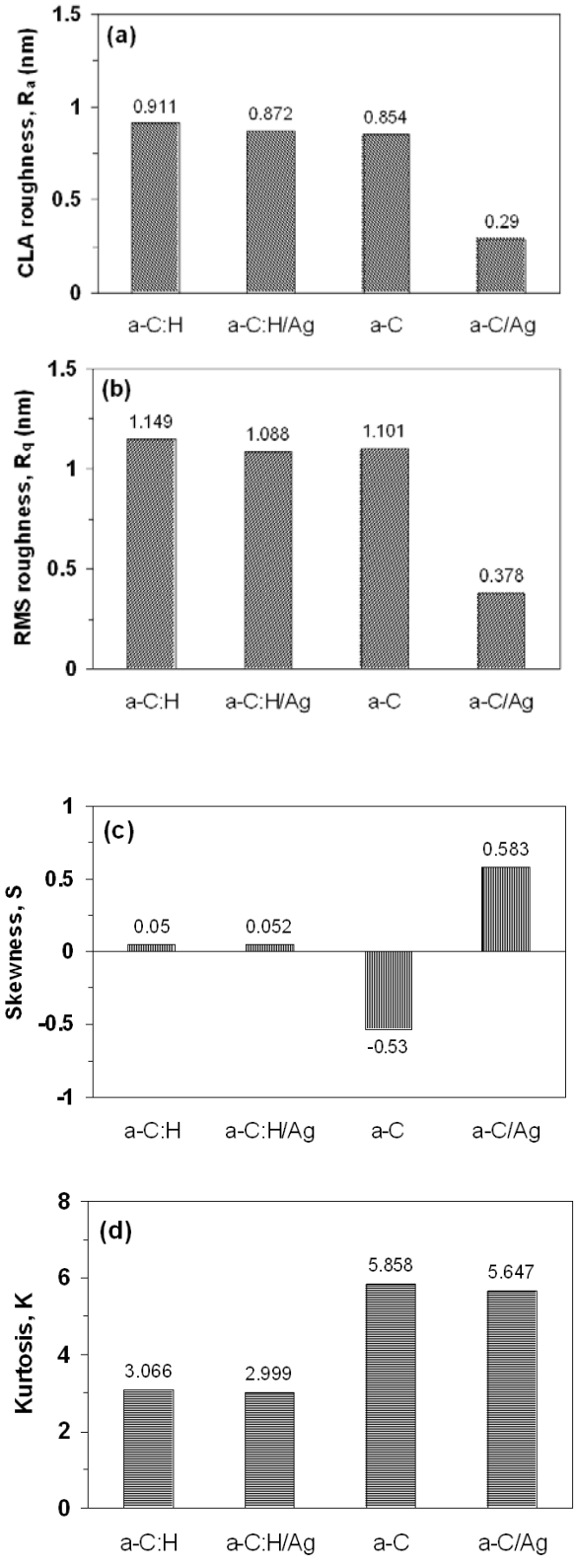
(a)
CLA roughness, R_a (nm)
1.5
1
0.5
0
0.911
0.872
0.854
0.29
a-C:H
a-C:H/Ag
a-C
a-C/Ag
(b)
RMS roughness, R_q (nm)
1.5
1
0.5
0
1.149
1.088
1.101
0.378
a-C:H
a-C:H/Ag
a-C
a-C/Ag
(c)
Skewness, S
1
0.5
0
-0.5
-1
0.05
0.052
-0.53
0.583
a-C:H
a-C:H/Ag
a-C
a-C/Ag
(d)
Kurtosis, K
8
6
4
2
0
3.066
2.999
5.858
5.647
a-C:H
a-C:H/Ag
a-C
a-C/Ag

Figure 4

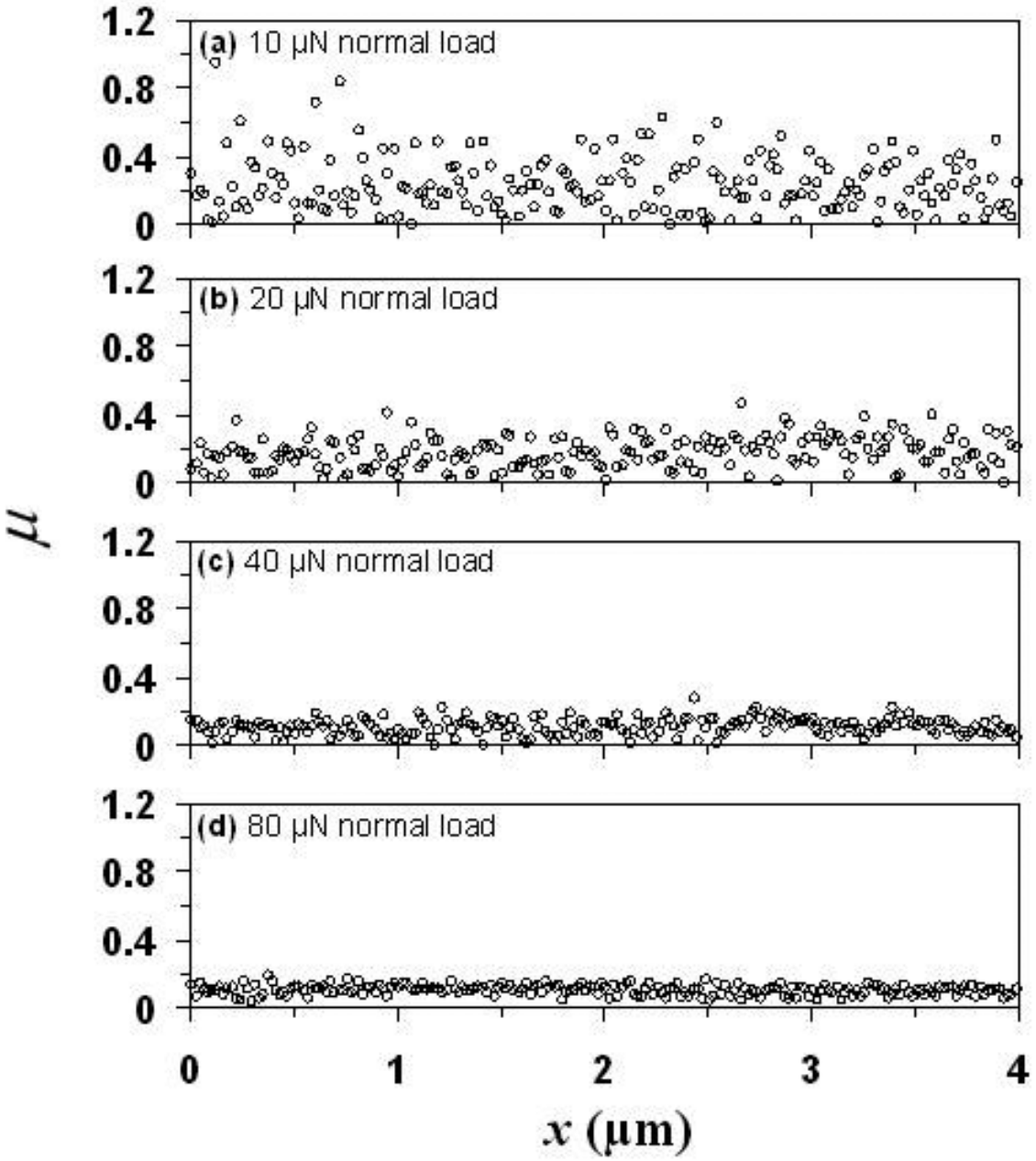
(a) 10 μN normal load
(b) 20 μN normal load
(c) 40 μN normal load
(d) 80 μN normal load
μ
1.2
0.8
0.4
0
0
1
2
3
4
x (μm)

Figure 5

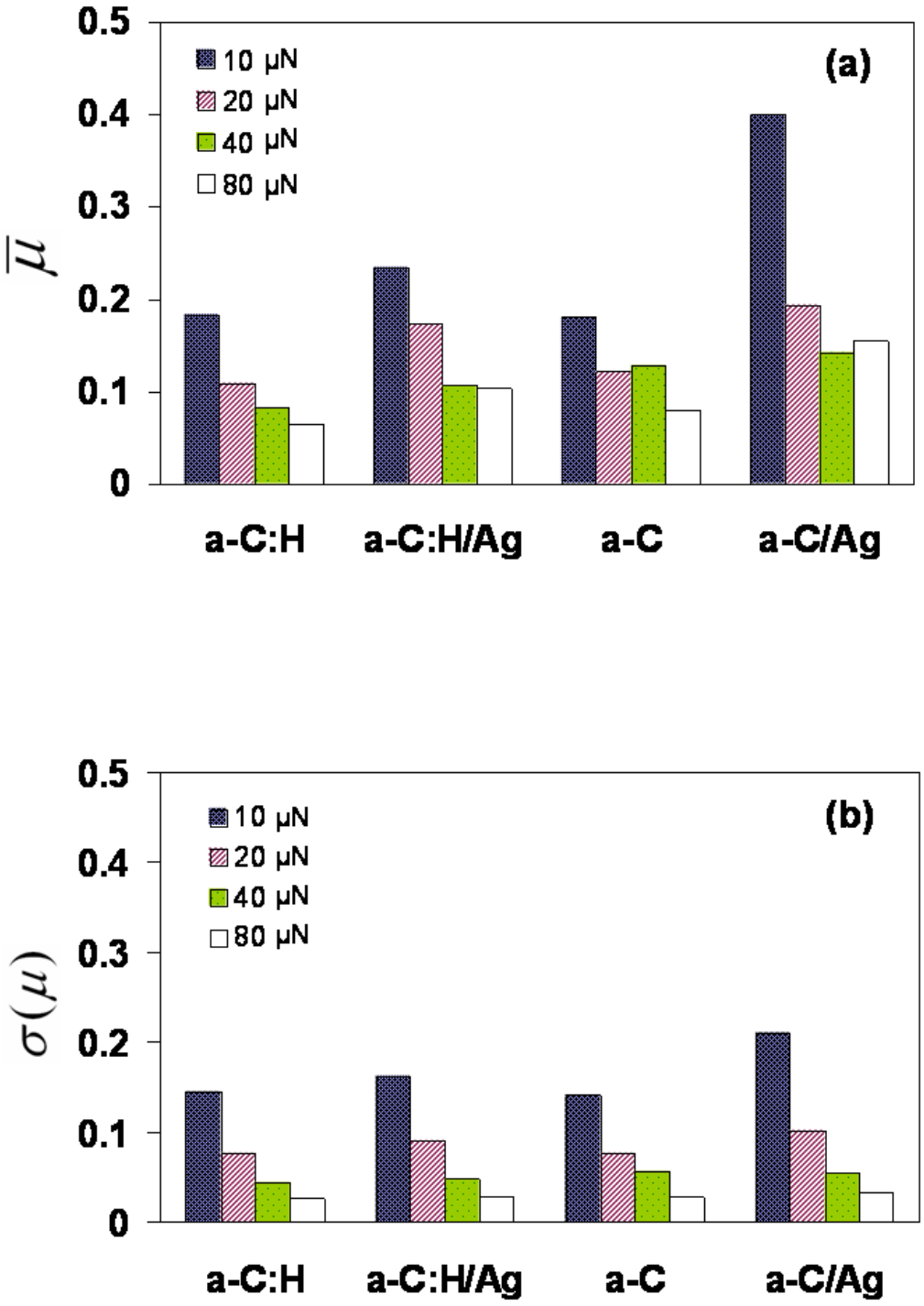
0.5
0.4
0.3
0.2
0.1
0
$\overline{\mu}$
10 μN
20 μN
40 μN
80 μN
(a)
a-C:H
a-C:H/Ag
a-C
a-C/Ag
0.5
0.4
0.3
0.2
0.1
0
$\sigma(\mu)$
10 μN
20 μN
40 μN
80 μN
(b)
a-C:H
a-C:H/Ag
a-C
a-C/Ag

Figure 6